ACS APPLIED ELECTRONIC MATERIALS

Article

Cite This: ACS Appl. Electron. Mater. XXXX, XXX, XXX−XXX

pubs.acs.org/acsaelm

n- Type Organic Field-Effect Transistors Based on Bisthienoisatin Derivatives

Dongho Yoo,*,† Xuyi Luo,‡ Tsukasa Hasegawa,† Minoru Ashizawa,*,† Tadashi Kawamoto,† Hiroyasu Masunaga,§ Noboru Ohta,§ Hidetoshi Matsumoto,† Jianguo Mei,‡ and Takehiko Mori*,†

†Department of Materials Science and Engineering, Tokyo Institute of Technology, O-okayama 2-12-1, Meguro-ku, Tokyo 152-8552, Japan

‡Department of Chemistry, Purdue University, West Lafayette, Indiana 47907, United States

§Japan Synchrotron Radiation Research Institute (JASRI/SPring-8), 1-1-1 Kouto, Sayo-cho, Sayo-gun, Hyogo 679-5198, Japan

*Supporting Information

ABSTRACT: Bisthienoisatins (BTI-R with R = n-propyl, n-hexyl, and 2-ethylhexyl) and the dicyanomethylene derivatives (BTICN-R) are prepared, and the thin-film transistors are investigated. The crystals have uniform stacking structures, but the packing pattern of the stacks varies depending on the alkyl chains. These materials show n-type transistor properties, and BTICNs exhibit greater performance than BTIs in general. In particular, BTICN-EH shows the maximum electron mobility exceeding 0.2 $cm^2 V^{-1} s^{-1}$.

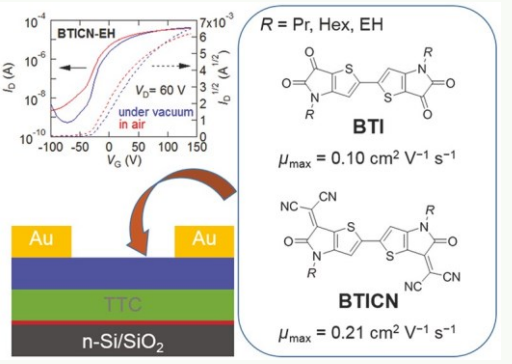

KEYWORDS: organic field-effect transistors, n-type transistors, indigo, isoindigo, thienoisoindigo, bisthienoisatin, dicyanomethylene

INTRODUCTION

In recent years organic semiconductors (OSCs) are investigated extensively because of the potential applications to the low-cost and simple fabrication of large-area electronic devices for photovoltaics,[1,2] light-emitting diodes,[3] and organic field-effect transistors (OFET).[4−8] There remains, however, a lot of room for improving n-type OSCs, where the development of device performance and stability in air have delayed in comparison with p-type OSCs. Many of n-type OSCs are still unstable when operated in air; this is ascribed to the lowest unoccupied molecular orbital (LUMO) levels which are not sufficiently low.[9] Therefore, enormous efforts have been dedicated to develop air-stable n-type OSCs.[10,11] Among n-type OSCs, diketopyrrolopyrrole,[12,13] naphthalene diimide,[14−18] benzothiadiazole,[19,20] and isoindigo are representative units used not only in acceptor parts of donor−acceptor polymers but also in small-molecule semiconductors.[21−24] Like these units, introduction of strong electron-withdrawing groups, such as carbonyl groups,[12−18,21−25] diimide groups,[14−18] thiadiazole groups,[19,20] and cyano groups,[26−28] is an effective approach for designing novel n-type OSCs.

Bisisoindigo is a representative electron-deficient unit used in n-type OSCs.[29] Bisisatin (Scheme 1) is a synthetic precursor of bisisoindigo and also a promising n-type organic material due to the planar framework with four electron-withdrawing carbonyl groups. Moreover, when the β-position carbonyl group is modified by a dicyanomethylene group, we can further lower the LUMO levels to obtain potentially air-stable n-type materials.[26−28] To date, two types of bisisatin derivatives have been reported: one has a fused ring system with naphthalene core (Scheme 1a),[26] and another is bridged by a central single bond (Scheme 1b).[27] However, the latter takes a nonplanar structure twisted around the central single bond when the β-

Scheme 1. (a) Fused[26] and (b) Bridged Bisisatines;[27] (c) Prepared Thienobisisatin and (d) Dicyanomethylene Derivatives, Where R = n-Propyl (Pr), n-Hexyl (Hex), and 2-Ethylhexyl (EH)

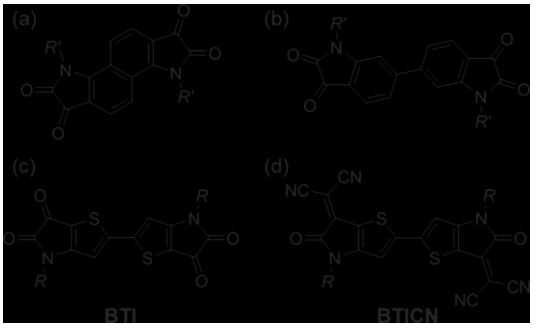

Received: February 20, 2019
Accepted: April 15, 2019
Published: April 15, 2019

DOI: 10.1021/acsaelm.9b00105
ACS Appl. Electron. Mater. XXXX, XXX, XXX−XXX

Scheme 2. Synthetic Scheme to BTI and BTICN

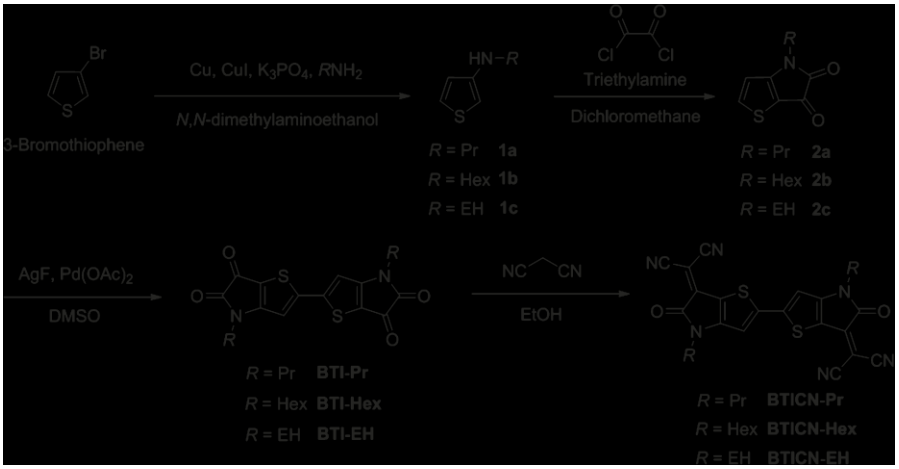

carbonyl groups are replaced with dicyanomethylene groups similarly to Scheme 1d, and this nonplanar framework is not preferable for OFET devices. Therefore, we have designed bisthienoisatin (BTI, Scheme 1c), where the benzene ring of bisisatin is replaced with a thiophene to maintain the perfect planarity. Herein, along with BTI, we have newly synthesized BTICN, in which β-carbonyl groups of BTI are substituted with dicyanomethylene groups (Scheme 1). BTI and BTICN are expected to make intermolecular S···O and S···S interactions suitable for carrier transport in OFETs, similarly to our previously reported thienoisoindigo.[25] We have prepared BTI and BTICN bearing different alkyl chains (R) at the N-position to investigate the effect to the molecular packing and the OFET performance. Because we have found difficulty in preparing R = methyl and ethyl derivatives, we have examined R = n-propyl (Pr), n-hexyl (Hex), and 2-ethylhexyl (EH) derivatives to improve solubility and crystallinity in addition to close intermolecular interactions realized by alkyl chain arrangement at the same time. In this paper, we report preparation and OFET properties of these BTI and BTICN materials.

EXPERIMENTAL SECTION

BTI and BTICN were prepared according to Scheme 2. From 3-bromothiophene, thienoisatin (2a− 2c) was prepared according to a previous report.[28] By oxidative coupling with silver fluoride as an oxidizing reagent and palladium acetate as a catalyst, BTIs were synthesized using the optimized condition in refs 30 and 31. Finally, BTIs were treated with malononitrile in ethanol via the Knoevenagel condensation reaction to afford BTICNs as the desired compounds.[26,27] All compounds were purified by sublimation before device fabrication.

OFETs were fabricated by thermal deposition of organic active layers (50 nm) onto tetratetracontane ($C_{44}H_{90}$, TTC, ε = 2.5)-modified (20 nm) SiO_2 (300 nm, C = 11.5 nF/cm^2)/n-doped Si substrates,[32− 34] where the calculated overall capacitance of the gate dielectrics was 10.4 nF/cm^2.[35] Then, the top-contact Au electrodes were thermally deposited using a shadow metal mask; the channel length (L) and width (W) were 100 and 1000 μm, respectively. The OFET properties were measured under the vacuum of 10^{-3} Pa and in air by using a Keithley 4200 semiconductor parameter analyzer. The field-effect mobility (μ) and threshold voltage (V_T) were calculated in the saturation regime by using the equation $I_{DS} = \mu(WC_i/2L)(V_G - V_T)^2$, where I_{DS} and V_G are the drain current and gate voltage, respectively. Then, μ was extracted from the slope where the $\sqrt{I_{DS}}$ vs V_G plot was straight.

The density functional calculations were performed with the B3LYP* functional and TZP basis set using ADF software.[36]

RESULTS AND DISCUSSION

Electronic Properties. The frontier orbital energy levels were investigated by cyclic voltammetry and the absorption spectra (Figure 1). BTIs and BTICNs in dichloromethane

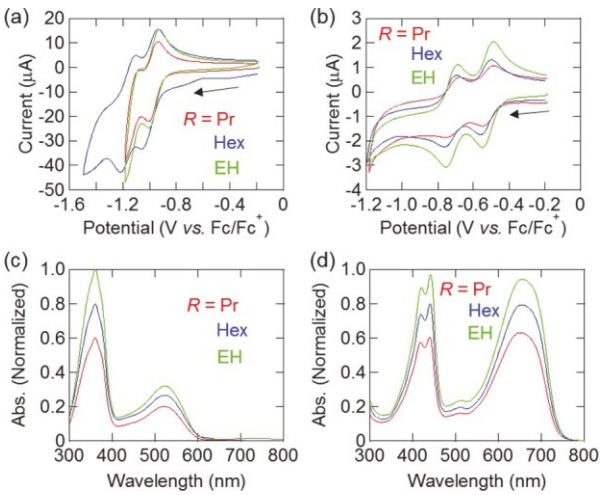

Figure 1. Cyclic voltammograms of (a) BTIs and (b) BTICNs. UV− vis absorption spectra of (c) BTIs and (d) BTICNs in DCM solutions.

(DCM) exhibited two reversible reduction waves, and the LUMO levels were estimated from the first reduction half-wave potentials ($E_{1/2}$).[37] As shown in Table 1, the LUMO levels of BTIs are located at − 3.80 eV or slightly below and the LUMO levels of BTICNs are located below − 4.25 eV, indicating the electron-withdrawing ability of the dicyanomethylene part is strong enough to achieve air-stable n-type OFET properties.[9,38] The optical gaps (E_g^{opt}) are estimated from λ_{onset} of the DCM solution absorption spectra. A bathochromic shift of ~ 140 nm is observed from BTIs to BTICNs due to the electron-withdrawing dicyanomethylene groups (Figure 1c,d). Also, in comparison with the solution spectra, the absorption bands of thin films are shifted to long wavelengths because of the intermolecular interactions in the solid state (Figure S1). From the LUMO levels and the optical gaps, the highest

DOI: 10.1021/acsaelm.9b00105

Table 1. Summary of Electrochemical and Optical Properties

compd	alkyl (R)	$E_{1/2}$ (V)	E_{LUMO} (eV)	λ_{onset} (nm)	λ_{max} (nm)	E_g^{opt} (eV)	E_{HOMO} (eV)
BTI	Pr	−0.973	−3.83	597	360, 521	2.08	−5.91
	Hex	−1.00	−3.80	601	360, 522	2.06	−5.86
	EH	−0.968	−3.83	600	361, 524	2.06	−5.89
BTICN	Pr	−0.521	−4.28	738	418, 439, 652	1.68	−5.96
	Hex	−0.530	−4.27	721	418, 440, 653	1.72	−5.99
	EH	−0.519	−4.28	743	420, 441, 655	1.67	−5.95

occupied molecular orbital (HOMO) levels of BTIs and BTICNs are estimated to be slightly above −6.0 eV (Table 1).

Crystal Structures. Crystal data of BTI-Pr, BTI-Hex, and BTICN-EH are summarized in Table 2, and lattice constants

Table 2. Crystallographic Data of BTI-Pr, BTI-Hex, and BTICN-EH

	BTI-Pr	BTI-Hex	BTICN-EH
chemical formula	$C_{18}H_{16}N_2O_4S_2$	$C_{24}H_{28}N_2O_4S_2$	$C_{34}H_{36}N_6O_2S_2$
formula weight	388.46	472.62	624.82
crystal system	triclinic	monoclinic	monoclinic
space group	P−1	C2/c	C2/c
a (Å)	4.96243(19)	33.028(3)	31.6727(7)
b (Å)	7.6511(3)	5.02936(18)	6.81282(16)
c (Å)	12.2057(5)	14.9494(5)	15.1228(4)
α(deg)	102.765(3)	90	90
β(deg)	92.376(2)	111.402(3)	92.1448(14)
γ(deg)	106.291(3)	90	90
V (Å^3)	431.17(3)	2312.0(2)	3260.91(13)
Z	1	4	4
total refls	5044	12385	18191
unique refls (R_{int})	1548 (0.0890)	2079 (0.0569)	2949 (0.0508)
D_{calc} (g/cm^3)	1.496	1.358	1.273
R_1[a]	0.0654	0.0562	0.0900
R_w[b]	0.1566	0.1560	0.3079
GOF	0.964	1.089	1.198
T (K)	212	171	104

[a]$R_1[F^2 > 2\sigma(F^2)]$. [b]$wR_2(F^2)$ for all observed reflections.

of BTICN-Hex are described in the Supporting Information. BTI-Pr crystallizes in a triclinic system with the space group P−1, and the half molecule is crystallographically independent. BTI-Hex and BTICN-EH make basically isostructural crystals having a monoclinic system with the space group C2/c, in which the half molecule is crystallographically independent. These molecules are located on inversion centers, and the molecular cores adopt a perfectly planar geometry.

In BTI-Pr, the alkyl chains are extending approximately perpendicular to the BTI plane (Figure 2a,b). The molecules form a uniform stacking structure along the a axis with the interplanar spacing of 3.36 Å (Figure 2b). The stacked molecules are slipped along the molecular long axis (Figure 2c), so that a thienoisatin group is located in between the two thienoisatin groups of the adjacent molecule. Because the sulfur atoms are oriented alternately upward and downward, there is no short S···S contact in the stacks. The adjacent columns are parallel to each other, so that all molecules are parallel (Figure 2d). Along the intercolumnar (b) axis, an intermolecular S···S interaction with the distance of 3.44 Å is observed (Figure 2d). In addition, a hydrogen bond O···H with the distance of 2.31 Å is observed between the oxygen

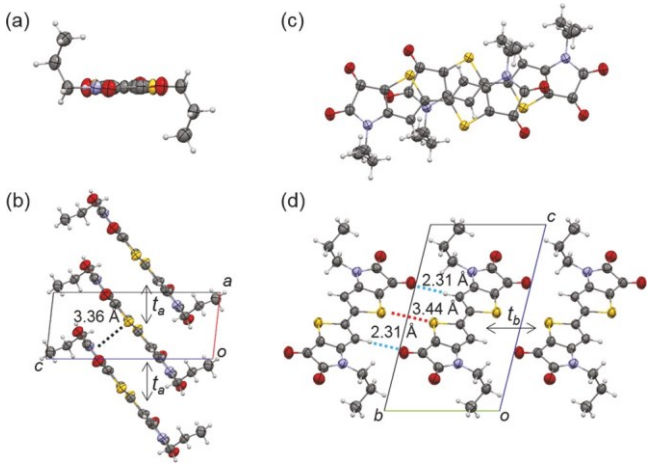

Figure 2. (a) Molecular structure of BTI-Pr viewed along the molecular long axis. (b) Crystal structure viewed along the b axis. (c) Molecular overlap mode viewed perpendicular to the molecular plane. (d) Crystal structure viewed along the a axis.

atom of the carbonyl group and the hydrogen atom of the thiophene along the intercolumnar (b) axis.

In BTI-Hex, the hexyl chains are extending nearly within the BTI core, which are tilted only ~24.5° from the molecular plane (Figure 3a). The molecules are uniformly stacked along the b axis with the interplanar distance of 3.32 Å (Figure 3b). The molecular overlap mode is similar to BTI-Pr (Figure 3c). The adjacent columns are, however, tilted in opposite directions by making an angle of 82.6° (Figure 3d). Nonetheless, the adjacent chains are connected by an S···S short contact with the distance of 3.47 Å (Figure 3e). In addition, the adjacent chains are connected by hydrogen bonds with the distance of 2.33 Å for C⊕ O···H− thiophene. Accordingly, BTI-Pr and BTI-Hex construct a pseudo-two-dimensional conduction path because of the intermolecular S···S interactions between the columns.

BTICN-EH is basically isostructural to BTI-Hex, though the alkyl chains are more tilted (29.8°) from the molecular plane (Figure 4a). The molecules are uniformly stacked along the b axis with the interplanar distance of 3.40 Å (Figure 4b). The stacked molecules are slipped not only along the molecular long axis but also along the molecular short axis. Accordingly, the thiophene sulfur sides of thienoisatin groups overlap with each other in an eclipsed manner (Figure 4c). In addition, a nitrogen atom of dicyanomethylene groups is placed on the top of a thiophene ring. Similarly to BTI-Hex, the adjacent columns are tilted in opposite directions by making an angle of 59.9° (Figure 4d). However, BTICN-EH does not have any short S···S contact, though the adjacent chains are connected by hydrogen bonds with the distance of 2.51 Å for C⊖ N···H− thiophene (Figure 4e). The absence of any short S···S contact is related to the introduction of the dicyanomethylene groups,

DOI: 10.1021/acsaelm.9b00105
ACS Appl. Electron. Mater. XXXX, XXX, XXX−XXX

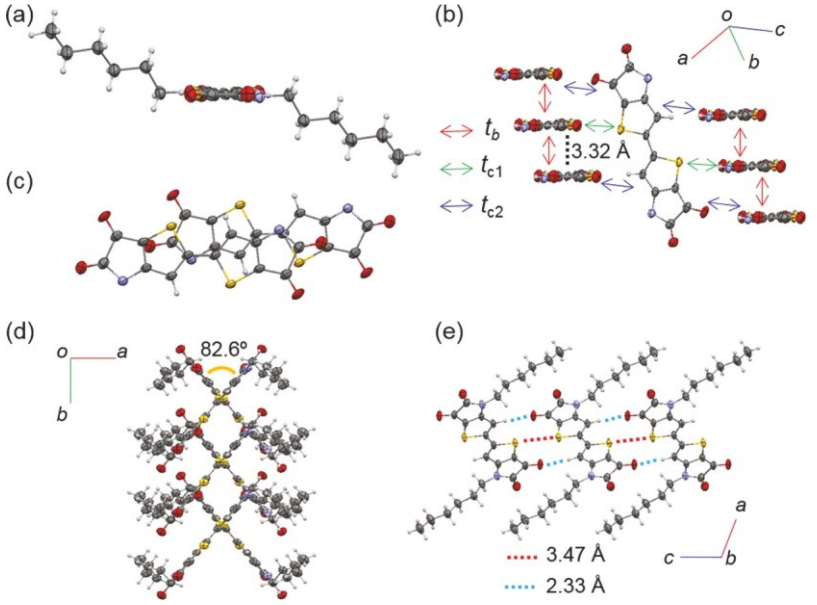

Figure 3. (a) Molecular structure of BTI-Hex viewed along the molecular long axis. (b) Structure of columns viewed along the molecular long axis. (c) Molecular overlap mode viewed perpendicular to the molecular plane. (d) Crystal structure viewed along the molecular short axis and (e) along the b axis. For clarification, the alkyl groups are omitted in (b) and (c).

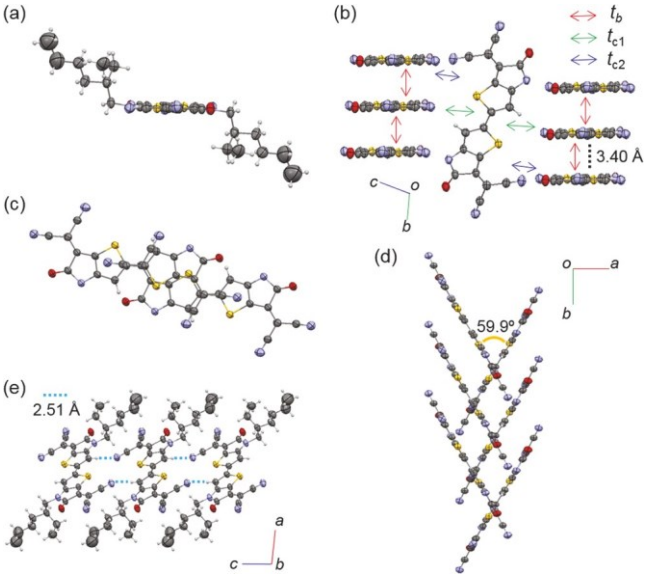

Figure 4. (a) Molecular structure of BTICN-EH viewed along the molecular long axis. (b) Structure of columns viewed along the molecular long axis. (c) Molecular overlap mode viewed perpendicular to the molecular plane. (d) Crystal structure viewed along the molecular short axis and (e) along the b axis. For clarification, the alkyl groups are omitted in (b), (c), and (d).

which block the side-by-side contacts. As a result, the conduction path is confined in the one-dimensional columnar direction.

The difference of the conduction path is investigated by calculating the transfer integrals for electrons (Table 3).[39,40] The stacking direction is the a axis in BTI-Pr, whereas the b axis in BTI-Hex and BTICN-EH. BTI-Pr has comparable intrachain (//a) and interchain (//b) transfers, and the anisotropy is less than three in BTI-Hex. However, BTICN-EH has a large transfer only along the stacks (//b). This is entirely in agreement with the absence of interchain S···S interactions. Nonetheless, BTICN-EH has a very large intrachain transfer because of the characteristic overlap mode (Figure 4c). The reorganization energy (λ) of BTICN (221 meV) is considerably smaller than that of BTI (338 meV). The resulting calculated mobility of BTICN-EH is significantly larger than those of BTI-Pr and BTI-Hex.[41]

Thin Film Properties. To evaluate thin-film surface morphologies and microstructures, X-ray diffraction (XRD) and grazing-incidence wide-angle X-ray scattering (GIWAXS) were performed (Figure 5). BTIs and BTICNs show sharp XRD peaks (Figure 5a,b), where the extracted d values are summarized in Table 4. The out-of-plane d-spacings observed in GIWAXS (Figure 5c−h) are in good agreement with the XRD results. Many sharp GIWAXS peaks are observed particularly in BTICN-R, reflecting the highly crystalline nature of the thin films. We have observed π−π stacking peaks at around 3.7 Å (q_{xy} = 1.69−1.72 $Å^{-1}$) and 4.1 Å (q_{xy} = 1.52−1.55 $Å^{-1}$). Another peak appears around 7.5 Å (q_{xy} = 0.83−0.86 $Å^{-1}$) in BTI-Pr, BTI-Hex, BTI-EH, and BTICN-EH as well as around 9.2 Å (q_{xy} = 0.68−0.69 $Å^{-1}$) in BTICN-Pr and BTICN-Hex (Table 4), which are attributable to the interchain periodicity. The π−π peaks around 3.7 Å coincide

Table 3. Electron Transfer Integrals, Reorganization Energies, and Calculated Mobilities

compd	t_a (meV)	t_b (meV)	t_c (meV)	λ (meV)	μ_{cal} (cm^2 V^{-1} s^{-1})
BTI-Pr	−65.0	−56.9		338	0.031
BTI-Hex		−60.4	24.5 (t_{c1}), −5.1 (t_{c2})	338	0.028
BTICN-EH		−163.6	−6.2 (t_{c1}), −5.8 (t_{c2})	221	0.84

DOI: 10.1021/acsaelm.9b00105
ACS Appl. Electron. Mater. XXXX, XXX, XXX−XXX

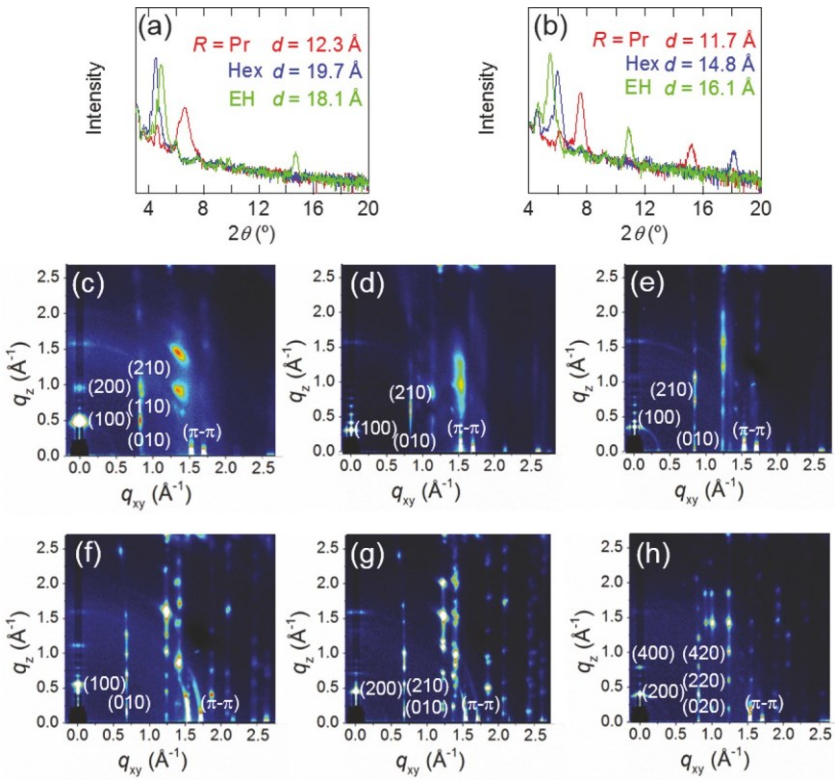

Figure 5. XRD patterns of (a) BTIs and (b) BTICNs. GIWAXS patterns of (c) BTI-Pr, (d) BTI-Hex, (e) BTI-EH, (f) BTICN-Pr, (g) BTICN-Hex, and (h) BTICN-EH. (100) and (200) indicate the interlayer reflections, and (010) and (020) designate the interchain reflections.

Table 4. XRD and GIWAXS d-Values (Å)

			-Pr	-Hex	-EH
BTI	XRD	⊥	12.3	19.7	18.1
	GIWAXS	⊥	12.1	19.6	18.2
		π- π	3.66, 4.13	3.69, 4.07	3.68, 4.13
		interchain	7.35	7.48	7.38
BTICN	XRD	⊥	11.7	14.8	16.1
	GIWAXS	⊥	11.6	14.8	15.7
		π- π	3.69, 4.07	3.71, 4.11	3.69, 4.05
		interchain	9.15	9.20	7.55

with half of these interchain periodicities in BTI-Pr, BTI-Hex, BTI-EH, and BTICN-EH, but even BTICN-Pr and BTICN-Hex show the 3.7 Å peaks.

In BTI-Pr, the out-of-plane d-spacing (12.1 Å, $q_z = 0.52$ Å^{-1}) is very close to c sin α sin β(11.9 Å), indicating the molecules are standing perpendicular to the substrate. The interchain peak observed at 7.35 Å is consistent with crystallographic b axis (7.65 Å). These observations indicate that the crystallographic ab plane is aligned parallel to the substrate (Figure S5). The molecular tilt angle is 45.8° from the substrate normal. The crystal structure of BTICN-Pr is unknown, but the XRD

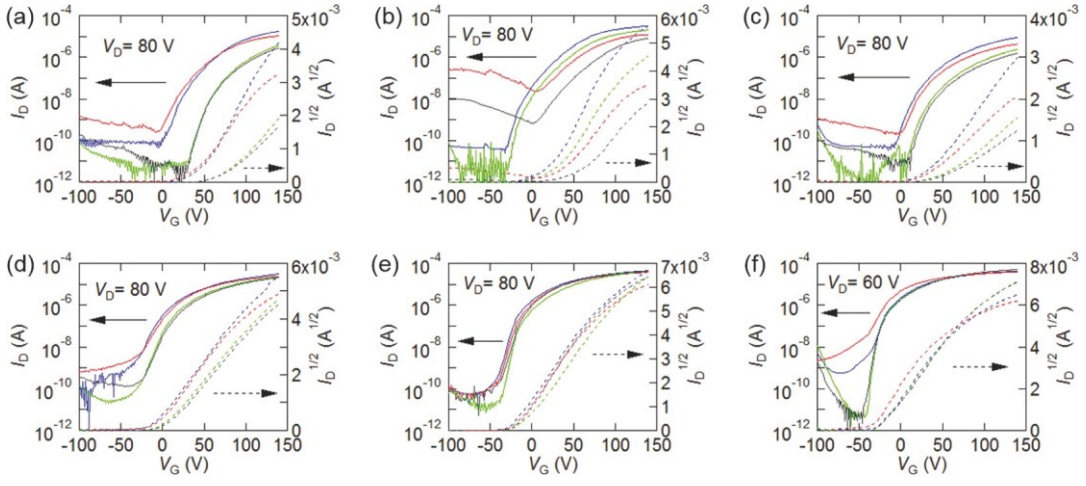

Figure 6. Transfer characteristics of (a) BTI-Pr, (b) BTI-Hex, (c) BTI-EH, (d) BTICN-Pr, (e) BTICN-Hex, and (f) BTICN-EH. The blue and red curves are for pristine samples measured under vacuum and in air, respectively. The green and black curves are measured after 150 days under vacuum and in air.

DOI: 10.1021/acsaelm.9b00105
ACS Appl. Electron. Mater. XXXX, XXX, XXX- XXX

pattern suggests the thin-film structure is basically the same as BTI-Pr.

The out-of-plane d-spacing of BTI-Hex (19.6 Å, q_z = 0.32 Å^{-1}) is considerably larger than a/2 (16.5 Å) and c (14.9 Å). In contrast to BTI-Pr, alkyl chains of BTI-Hex are extending not perpendicular to the molecular plane but perpendicular to the molecular long axis (Figure 3a,e). If the alkyl chains are assumed to be approximately perpendicular to the substrate, the molecular length is estimated to be 19.4 Å (Figure S6). This is in good agreement with the observed XRD, but the molecular core has to take the side-on arrangement. This packing pattern is entirely different from the other compounds, so we could not exclude the possibility that the thin-film structure is different from the crystal structure. In such a case, the alkyl chain orientation and the crossing stacks are potentially different from the crystal. Because BTI-EH has similar XRD patterns, BTI-EH is expected to have a similar molecular packing to BTI-Hex.

The thin-film structure of BTICN-Hex is consistent with the crystal lattice (Supporting Information). The out-of-plane d-spacing (14.8 Å, q_z = 0.43 Å^{-1}) is close to (1/2) c sin(β)) (14.5 Å), and the interchain spacing (9.20 Å) is in agreement with the crystallographic a axis (9.22 Å). These observations indicate that the crystallographic ab plane is aligned parallel to the substrate (Figure S7). Therefore, the molecular tilt angle from the substrate normal is 48.8°.

Transistor Properties. BTIs and BTICNs exhibit n-type transistor characteristics under vacuum and in air. Transfer characteristics are shown in Figures 6, and the transistor properties are summarized in Table 5. In general, the n-propyl derivatives tend to show smaller mobilities than the other two, and BTICN exhibits higher performance than BTI. BTI-Pr and BTI-Hex show electron mobilities in the 10^{-2} cm^2 V^{-1} s^{-1} order (Figure 6a,b), in agreement with the calculated mobility (Table 3). However, the mobility of BTI-EH drops to the 10^{-3} cm^2 V^{-1} s^{-1} order (Figure 6c). The highest electron mobility (μ_{max}) is 0.10 cm^2 V^{-1} s^{-1} in BTI-Hex.

Upon air exposure, mobilities of the BTIs transistors decrease to typically half (Table 5), and the off current increases compared to the operation under vacuum (Figure 6a−c). In particular, the off current of BTI-Hex increases considerably. However, the transfer characteristics of BTI-Pr and BTI-EH do not largely change in the logarithmic scale. This moderate air stability is consistent with the comparatively high LUMO levels around −3.8 eV (Table 1).

Under vacuum, BTICNs exhibit electron mobilities in the order of 10^{-1}–10^{-2} cm^2 V^{-1} s^{-1} with the on/off ratios up to 10^6. BTICNs show negative V_T, indicating the normally on properties (Figure 6d−f). Normally on transistors are not many in n-type transistors,[10] but this is associated with the strong acceptor ability of BTICN with the LUMO levels around −4.28 eV. The normally on property is closely related to the bulk conductivity. The electrical resistance of BTICN-EH, estimated by the two-probe method using a 50 nm thin film, is 16 MΩ, so the resulting conductivity amounts to 1.3 × 10^{-3} S cm^{-1}. In Figure 6f, I_D = 10^{-5} A at V_G = 0 V leads to 6 MΩ and similar conductivity. However, the off current in the negative V_G region affords 3.3 × 10^{-7} S cm^{-1}. This reminds us transport observed at the interface of two OSCs.[42,43] The mobility increases in the order of BTICN-Pr < BTICN-Hex < BTICN-EH, and μ_{max} is 0.21 cm^2 V^{-1} s^{-1} in BTICN-EH. This is consistent with the large calculated mobility (0.82 cm^2 V^{-1} s^{-1} in Table 3), which is associated with the large transfer integral (164 meV) as well as the comparatively small reorganization energy. In air, μ and V_T do not change largely, so that these transistors are operated stably in air as expected from the LUMO levels.

Table 5. OFET Properties of the Thin-Film Transistors

compound	conditions	measurements	μ_{av} [μ_{max}] (cm^2 V^{-1} s^{-1})	V_T (V)	I_{on}/I_{off}
BTI-Pr	pristine	under vacuum	0.042 [0.058]	44	10^5
		in air	0.025 [0.037]	38	10^4
	after 150 days	under vacuum	0.016 [0.022]	73	10^5
		in air	0.011 [0.019]	72	10^5
BTI-Hex	pristine	under vacuum	0.082 [0.10]	22	10^5
		in air	0.029 [0.041]	31	10^3
	after 150 days	under vacuum	0.044 [0.052]	26	10^6
		in air	0.026 [0.033]	55	10^4
BTI-EH	pristine	under vacuum	0.015 [0.022]	32	10^5
		in air	7.2 × 10^{-3} [9.9 × 10^{-3}]	29	10^4
	after 150 days	under vacuum	5.9 × 10^{-3} [7.4 × 10^{-3}]	45	10^6
		in air	2.9 × 10^{-3} [4.1 × 10^{-3}]	42	10^5
BTICN-Pr	pristine	under vacuum	0.035 [0.061]	−14	10^5
		in air	0.034 [0.057]	−7	10^4
	after 150 days	under vacuum	0.026 [0.053]	1	10^6
		in air	0.022 [0.043]	6	10^5
BTICN-Hex	pristine	under vacuum	0.070 [0.11]	−22	10^6
		in air	0.061 [0.090]	−19	10^6
	[illegible]	[illegible]	[illegible]	[illegible]	[illegible]
		in air	0.10 [0.19]	−24	10^6

The long-term stability was investigated by measuring the transistor properties after 150-day storage in air (Figure 6a−f and Table 5). Mobilities of BTIs drop evidently after 150 days (Table 5), and the positions of the green and black curves are considerably different from the blue and red ones (Figure 6a−c). Those of BTICNs are, however, almost unchanged; this is evident that the green and black curves do not move from the original ones (Figure 6d−f). BTICNs show long-term stability even in the thin-film transistors, but BTIs degrade gradually in the ambient conditions. Shifts of V_T are particularly notable in BTI-Pr and BTICN-Pr. In BTI and BTICN with hexyl and 2-ethylhexyl groups, a large shift of V_T is not observed after the long-term storage. One of the reasons is the passivation effect of the alkyl chain;[44] the propyl groups are too short to achieve passivation effect, but the hexyl and 2-ethylhexyl groups are considered to work as passivation layers.

DOI: 10.1021/acsaelm.9b00105
ACS Appl. Electron. Mater. XXXX, XXX, XXX−XXX

CONCLUSIONS

In summary, we have investigated BTIs and BTICNs with such alkyl groups as n-propyl (Pr), n-hexyl (Hex), and 2-ethylhexyl (EH) for n-type OFETs. LUMO levels of BTIs and BTICNs are appropriate for electron transport, and particularly BTICNs have sufficiently deep LUMO levels suitable for air-stable n-type OFET operation. Single crystals of BTI-Pr, BTI-Hex, and BTICN-EH have uniform stacks of planar molecular cores, though the orientation of the alkyl chains and the packing pattern of the stacks are largely dependent on the alkyl chains. BTI-Pr and BTI-Hex have intercolumnar hydrogen bonds as well as intercolumnar S···S interactions, which realize the two-dimensional conduction path. By combining crystal structures with thin-film XRD and GIWAXS, molecular packing and molecular arrangement in the thin films are determined. Although these molecules are largely tilted (~ 50°) from the substrate normal, BTIs exhibit moderate electron mobilities, and BTICNs exhibit excellent n-type transistor characteristics with remarkable long-term air stability. In particular, BTICN-EH shows a maximum electron mobility of 0.21 $cm^2 V^{-1} s^{-1}$. This is consistent with the large calculated mobility, which comes from the large transfer integral and the small reorganization energy. BTI is a promising electron-accepting framework for OSC materials, and introduction of dicyano-methylene groups is an efficient way to improve the n-type OFET properties.

ASSOCIATED CONTENT

* Supporting Information

The Supporting Information is available free of charge on the ACS Publications website at DOI: 10.1021/acsaelm.9b00105.

Additional information for material synthesis, electrochemical properties and optical properties, DFT calculations, single crystal X-ray structure analyses, thin-film microstructures and morphologies, and thin-film transistor properties (PDF)

Crystal data (CIF)

Accession Codes

CCDC 1894811− 1894814 contain the supplementary crystallographic data for this paper.

AUTHOR INFORMATION

Corresponding Authors

*E-mail: yoo.d.aa@m.titech.ac.jp.

*E-mail: ashizawa.m.aa@m.titech.ac.jp.

*E-mail: mori.t.ae@m.titech.ac.jp.

ORCID

Dongho Yoo: 0000-0003-0886-7533

Tsukasa Hasegawa: 0000-0002-6311-2988

Minoru Ashizawa: 0000-0002-6810-256X

Hidetoshi Matsumoto: 0000-0002-4949-1184

Jianguo Mei: 0000-0002-5743-2715

Takehiko Mori: 0000-0002-0578-5885

Notes

The authors declare no competing financial interest.

ACKNOWLEDGMENTS

The authors are grateful to the Center for Advanced Materials Analysis, Tokyo Institute of Technology, for X-ray diffraction measurements. The authors also thank Professor Hidehiro Uekusa for using RIGAKU VM-spider. GIWAXS experiments were performed on BL40B2 at SPring-8 with the approval of the Japan Synchrotron Radiation Research Institute (JASRI) (Proposal No. 2018B1001). This work was partly supported by JPSJ KAKENHI Grants (16K13974 T.M., 17K05830 M.A., and 18H02044 T.M.) and the Takahashi Industrial and Economic Research Foundation. J.M. and X.L. acknowledge the financial support from the National Science Foundation (NSF CAREER Award, #1653909).

REFERENCES

(1) Brabec, C.; Scherf, U.; Dyakonov, V. Organic Photovoltaics: Materials, Device Physics, and Manufacturing Technologies, 2nd ed.; Wiley: Hoboken, NJ, 2016.

(2) Zhou, J.; Zuo, Y.; Wan, X.; Long, G.; Zhang, Q.; Ni, W.; Liu, Y.; Li, Z.; He, G.; Li, C.; et al. Solution-Processed and High-Performance Organic Solar Cells Using Small Molecules with a Benzodithiophene Unit. J. Am. Chem. Soc. 2013, 135, 8484− 8487.

(3) Friend, R. H.; Gymer, R. W.; Holmes, A. B.; Burroughes, J. H.; Marks, R. N.; Taliani, C.; Bradley, D. D. C.; Dos Santos, D. A.; Bredas, J. L.; Logdlund, M.; Salaneck, W. R. Electroluminescence in Conjugated Polymers. Nature 1999, 397, 121− 128.

(4) Bao, Z.; Locklin, J. Organic Field-Effect Transistors; CRC Press: New York, 2007.

(5) Murphy, A. R.; Frechet, J. M. J. Organic Semiconducting Oligomers for Use in Thin Film Transistors. Chem. Rev. 2007, 107, 1066− 1096.

(6) Klauk, H. Organic Thin-Film Transistors. Chem. Soc. Rev. 2010, 39, 2643− 2666.

(7) Wang, C.; Dong, H.; Hu, W.; Liu, Y.; Zhu, D. Semiconducting π-Conjugated Systems in Field-Effect Transistors: A Material Odyssey of Organic Electronics. Chem. Rev. 2012, 112, 2208− 2267.

(8) Dong, H.; Fu, X.; Liu, J.; Wang, Z.; Hu, W. 25th Anniversary Article: Key Points for High-Mobility Organic Field-Effect Transistors. Adv. Mater. 2013, 25, 6158− 6183.

(9) Zhou, K.; Dong, H.; Zhang, H.; Hu, W. High Performance N-Type and Ambipolar Small Organic Semiconductors for Organic Thin Film Transistors. Phys. Chem. Chem. Phys. 2014, 16, 22448− 22457.

(10) Iijima, K.; Le Gal, Y.; Higashino, T.; Lorcy, D.; Mori, T. Birhodanines and Their Sulfur Analogues for Air-Stable n-Channel Organic Transistors. J. Mater. Chem. C 2017, 5, 9121− 9127.

(11) Iijima, K.; Le Gal, Y.; Lorcy, D.; Mori, T. Impact of Bulky Phenylalkyl Substituents on the Air-Stable n-Channel Transistors of Birhodanine Analogues. RSC Adv. 2018, 8, 18400− 18405.

(12) Qiao, Y.; Guo, Y.; Yu, C.; Zhang, F.; Xu, W.; Liu, Y.; Zhu, D. Diketopyrrolopyrrole-Containing Quinoidal Small Molecules for High-Performance, Air-Stable, and Solution-Processable n-Channel Organic Field-Effect Transistors. J. Am. Chem. Soc. 2012, 134, 4084− 4087.

(13) Iijima, K.; Mori, T. Electron Transport in Isodiketopyrrolopyrrole (IsoDPP). Chem. Lett. 2017, 46, 357− 359.

(14) Kakinuma, T.; Kojima, H.; Ashizawa, M.; Matsumoto, H.; Mori, T. Correlation of Mobility and Molecular Packing in Organic Transistors Based on Cycloalkyl Naphthalene Diimides. J. Mater. Chem. C 2013, 1, 5395− 5401.

(15) Chen, Z.; Zheng, Y.; Yan, H.; Facchetti, A. Naphthalenedicarboximide- vs Perylenedicarboximide-Based Copolymers. Synthesis and Semiconducting Properties in Bottom-Gate N-Channel Organic Transistors. J. Am. Chem. Soc. 2009, 131, 8− 9.

(16) Guo, X.; Kim, F. S.; Seger, M. J.; Jenekhe, S. A.; Watson, M. D. Naphthalene Diimide-Based Polymer Semiconductors: Synthesis, Structure− Property Correlations, and n-Channel and Ambipolar Field-Effect Transistors. Chem. Mater. 2012, 24, 1434− 1442.

(17) Hu, Y.; Gao, X.; Di, C.; Yang, X.; Zhang, F.; Liu, Y.; Li, H.; Zhu, D. Core-Expanded Naphthalene Diimides Fused with Sulfur Heterocycles and End-Capped with Electron-Withdrawing Groups for Air-Stable Solution-Processed n-Channel Organic Thin Film Transistors. Chem. Mater. 2011, 23, 1204− 1215.

DOI: 10.1021/acsaelm.9b00105

(18) Zhang, F.; Hu, Y.; Schuettfort, T.; Di, C.; Gao, X.; McNeill, C. R.; Thomsen, L.; Mannsfeld, S. C. B.; Yuan, W.; Sirringhaus, H.; et al. Critical Role of Alkyl Chain Branching of Organic Semiconductors in Enabling Solution-Processed N-Channel Organic Thin-Film Transistors with Mobility of up to 3.50 $Cm^2 V^{-1} s^{-1}$. J. Am. Chem. Soc. 2013, 135, 2338−2349.
(19) Wang, Y.; Hasegawa, T.; Matsumoto, H.; Mori, T.; Michinobu,
T. High-Performance n-Channel Organic Transistors Using High-Molecular-Weight Electron-Deficient Copolymers and Amine-Tailed Self-Assembled Monolayers. Adv. Mater. 2018, 30, 1707164.
(20) Hasegawa, T.; Ashizawa, M.; Aoyagi, K.; Masunaga, H.; Hikima, T.; Matsumoto, H. Thiadiazole-Fused Quinoxalineimide as an Electron-Deficient Building Block for N-Type Organic Semiconductors. Org. Lett. 2017, 19, 3275−3278.
(21) Ashizawa, M.; Masuda, N.; Higashino, T.; Kadoya, T.; Kawamoto, T.; Matsumoto, H.; Mori, T. Ambipolar Organic Transistors Based on Isoindigo Derivatives. Org. Electron. 2016, 35, 95−100.
(22) Lei, T.; Cao, Y.; Fan, Y.; Liu, C.-J.; Yuan, S.-C.; Pei, J. High-Performance Air-Stable Organic Field-Effect Transistors: Isoindigo-Based Conjugated Polymers. J. Am. Chem. Soc. 2011, 133, 6099−6101.
(23) Mei, J.; Kim, D. H.; Ayzner, A. L.; Toney, M. F.; Bao, Z. Siloxane-Terminated Solubilizing Side Chains: Bringing Conjugated Polymer Backbones Closer and Boosting Hole Mobilities in Thin-Film Transistors. J. Am. Chem. Soc. 2011, 133, 20130−20133.
(24) Stalder, R.; Mei, J.; Graham, K. R.; Estrada, L. A.; Reynolds, J. R. Isoindigo, a Versatile Electron-Deficient Unit For High-Performance Organic Electronics. Chem. Mater. 2014, 26, 664−678.
(25) Yoo, D.; Hasegawa, T.; Ashizawa, M.; Kawamoto, T.; Masunaga, H.; Hikima, T.; Matsumoto, H.; Mori, T. N-Unsubstituted Thienoisoindigos: Preparation, Molecular Packing and Ambipolar Organic Field-Effect Transistors. J. Mater. Chem. C 2017, 5, 2509−2512.
(26) Dhondge, A. P.; Tsai, P.-C.; Nien, C.-Y.; Xu, W.-Y.; Chen, P.-
M.; Hsu, Y.-H.; Li, K.-W.; Yen, F.-M.; Tseng, S.-L.; Chang, Y.-C.; et al. Angular-Shaped Naphthalene Bis(1,5-Diamide-2,6-Diylidene)-Malononitrile for High-Performance, Air-Stable N -Type Organic Field-Effect Transistors. Org. Lett. 2018, 20, 2538−2542.
(27) Dhondge, A. P.; Chen, J.-Y.; Lin, T.; Yen, F.-M.; Li, K.-W.;
Hsieh, H.-C.; Kuo, M.-Y. Di-2-(2-Oxindolin-3-Ylidene)Malononitrile Derivatives for N -Type Air-Stable Organic Field-Effect Transistors. Org. Lett. 2018, 20, 40−43.
(28) Dasari, R. R.; Dindar, A.; Lo, C. K.; Wang, C.-Y.; Quinton, C.; Singh, S.; Barlow, S.; Fuentes-Hernandez, C.; Reynolds, J. R.; Kippelen, B.; et al. Tetracyano Isoindigo Small Molecules and Their Use in N-Channel Organic Field-Effect Transistors. Phys. Chem. Chem. Phys. 2014, 16, 19345−19350.
(29) Randell, N. M.; Boutin, P. C.; Kelly, T. L. Bisisoindigo: Using a Ring-Fusion Approach to Extend the Conjugation Length of Isoindigo. J. Mater. Chem. A 2016, 4, 6940−6945.
(30) Luo, X.; Tran, D. T.; Sun, H.; Mi, T.; Kadlubowski, N. M.; Zhao, Y.; Zhao, K.; Mei, J. Bis-Isoindigos: New Electron-Deficient Building Blocks for Constructing Conjugated Polymers with Extended Electron Delocalization. Asian J. Org. Chem. 2018, 7, 2248−2253.
(31) Luo, X.; Tran, D. T.; Kadlubowski, N. M.; Ho, C. H. Y.; Riley, P.; So, F.; Mei, J. Side-Chain Sequence Enabled Regioisomeric Acceptors for Conjugated Polymers. Macromolecules 2018, 51, 8486−8492.
(32) Kraus, M.; Richler, S.; Opitz, A.; Brütting, W.; Haas, S.; Hasegawa, T.; Hinderhofer, A.; Schreiber, F. High-Mobility Copper-Phthalocyanine Field-Effect Transistors with Tetratetracontane Passivation Layer and Organic Metal Contacts. J. Appl. Phys. 2010, 107, 094503.
(33) Kraus, M.; Haug, S.; Brütting, W.; Opitz, A. Achievement of Balanced Electron and Hole Mobility in Copper-Phthalocyanine Field-Effect Transistors by Using a Crystalline Aliphatic Passivation Layer. Org. Electron. 2011, 12, 731−735.

(34) Opitz, A.; Horlet, M.; Kiwull, M.; Wagner, J.; Kraus, M.; Brütting, W. Bipolar Charge Transport in Organic Field-Effect Transistors: Enabling High Mobilities and Transport of Photo-Generated Charge Carriers by a Molecular Passivation Layer. Org. Electron. 2012, 13, 1614−1622.
(35) Baeg, K.-J.; Noh, Y.-Y.; Ghim, J.; Lim, B.; Kim, D.-Y. Polarity Effects of Polymer Gate Electrets on Non-Volatile Organic Field- Effect Transistor Memory. Adv. Funct. Mater. 2008, 18, 3678−3685.
(36) ADF2017.109; Scientific Computing & Modeling (SCM). Theoretical Chemistry; Vrije Universiteit, Amsterdam, The Nether- lands, https://www.scm.com.
(37) Tang, M. L.; Reichardt, A. D.; Wei, P.; Bao, Z. Correlating Carrier Type with Frontier Molecular Orbital Energy Levels in Organic Thin Film Transistors of Functionalized Acene Derivatives. J. Am. Chem. Soc. 2009, 131, 5264−5273.
(38) Usta, H.; Facchetti, A.; Marks, T. J. N-Channel Semiconductor Materials Design for Organic Complementary Circuits. Acc. Chem. Res. 2011, 44, 501−510.
(39) Prins, P.; Senthilkumar, K.; Grozema, F. C.; Jonkheijm, P.; Schenning, A. P. H. J.; Meijer, E. W.; Siebbeles, L. D. A. Charge Transport in Self-Organized π-Stacks of p-Phenylene Vinylene Oligomers. J. Phys. Chem. B 2005, 109, 18267−18274.
(40) te Velde, G.; Bickelhaupt, F. M.; Baerends, E. J.; Fonseca Guerra, C.; van Gisbergen, S. J. A.; Snijders, J. G.; Ziegler, T. Chemistry with ADF. J. Comput. Chem. 2001, 22, 931−967.
(41) Kojima, H.; Mori, T. Estimated Mobility of Ambipolar Organic Semiconductors, Indigo and Diketopyrrolopyrrole. Chem. Lett. 2013, 42, 68−70.
(42) Takahashi, Y.; Hayakawa, K.; Takayama, K.; Yokokura, S.; Harada, J.; Hasegawa, H.; Inabe, T. Charge Conduction Properties at the Contact Interface between (Phthalocyaninato)Nickel(II) and Electron Acceptor Single Crystals. Chem. Mater. 2014, 26, 993−998.
(43) Takahashi, Y.; Hasegawa, T.; Horiuchi, S.; Kumai, R.; Tokura, Y.; Saito, G. High Mobility Organic Field-Effect Transistor Based on Hexamethylenetetrathiafulvalene with Organic Metal Electrodes. Chem. Mater. 2007, 19, 6382−6384.
(44) Kurosawa, T.; Chiu, Y.-C.; Zhou, Y.; Gu, X.; Chen, W.-C.; Bao, Z. Impact of Polystyrene Oligomer Side Chains on Naphthalene Diimide-Bithiophene Polymers as n-Type Semiconductors for Organic Field-Effect Transistors. Adv. Funct. Mater. 2016, 26, 1261−1270.

DOI: 10.1021/acsaelm.9b00105